Stability Properties of Toroidal Alfvén Modes Driven by Fast Particles*

N. N. Gorelenkov, S. Bernabei, C. Z. Cheng, K. Hill, R. Nazikian, S. Kaye

Princeton Plasma Physics Laboratory, P.O. Box 451, Princeton, NJ 08543

Y. Kusama, G. J. Kramer, K. Shinohara, T. Ozeki

Japan Atomic Energy Research Institute, Mukouyama 801-1

Naka-machi, Naka-gun, Ibaraki-ken, 311-0193, Japan

M. V. Gorelenkova

TRINITI, Troitsk, Moscow Region, Russia, 142092

November 9, 1999

Abstract

In this report, the issues of Alfvén mode stability in advanced tokamak regimes are addressed based on recent developments in theory, computational methods, and progress in experiments. The instability of Toroidal Alfvén Eigenmodes (TAE) is analyzed for spherical tokamaks, such as the National Spherical Torus Experiment NSTX at the Princeton Plasma Physics Laboratory using the NOVA-K code.

Chirping modes in the Alfvén frequency range observed in JT-60U during the NNBI heating at energies $\mathcal{E}_{b0} = 360 keV$, and in the Tokamak Fusion Test Reactor (TFTR) at the Princeton Plasma Physics Laboratory during Ion Cyclotron Resonance Heating (ICRH) experiments, are analyzed using the kinetic nonperturbative code HINST,

which is able to resolve new resonant branches of the toroidal Alfvén modes called resonant TAE (RTAE). However, the chirping mechanism may be different for different experiments. In TFTR frequency chirping results from the slow variation of the q-profile between sawteeth. In Japan Atomic Energy Research Institute Tokamak (JT-60U) experiments some frequency chirping modes have very short time scale which suggests the cause is due to the change in the fast particle distribution.

1   Introduction

Within the Alfvén range of frequencies, many types of modes can be observed in experiments, including Toroidicity-induced Alfvén Eigenmodes (TAE)[1], which were seen in many experiments on tokamaks, such as the recent deuterium-tritium (D-T) experiments on the Tokamak Fusion Test Reactor (TFTR) at the Princeton Plasma Physics Laboratory[2]. Alfvén modes are believed to cause a degradation of fusion product confinement in a reactor, eventually terminating plasma burning. Other types of Alfvén modes are Beam-induced Alfvén Eigenmodes (BAE) with characteristic chirping mode frequency observed in regular tokamaks, such as DIII-D at General Atomics [3]. A new type of chirping frequency modes was reported in spherical tokamak experiments, such as those in START at Culham Laboratory in the United Kingdom[4], in TFTR[5] and Japan Atomic Energy Research Institute Tokamak (JT-60U)[6] devices, and in stellarators, such as the compact helical system (CHS) at National Institute for Fusion Science in Japan[7]. The common feature for these modes is the frequency chirping, which, however, may be very different in terms of physical mechanisms as can be seen from very different time scales of the chirping. Frequency chirping is a common phenomenon for experiments with strong fast particle pressure. The properties of Alfvén modes in the presence of a strong drive from fast particles is the subject of this paper. Theory has predicted that in the presence of a strong drive, TAEs will be strongly modified to new types of mode, the Resonant TAE[8] or Energetic Particle Modes (EPM)[9].

We will first study the effect of the strong drive of fast particles on TAEs in the National Spherical Tokamak Experiment (NSTX) at the Princeton Plasma Physics Laboratory[10], using well established numerical tools - ideal magnetohydrodynamics (MHD) code NOVA[11]. The fast particle effects on TAE stability are treated as perturbations in the kinetic code

NOVA-K[12][13]. The unique features of NSTX, such as low aspect ratio, high plasma and energetic particle beta, low Alfvén velocity with respect to beam ion injection velocity, and large Larmor radii present an entirely new regime for studying energetic particle physics. Proposed Neutral Beam Injection (NBI) and high harmonic Ion Cyclotron Resonance Heating (ICRH) in NSTX[10] will produce super Alfvénic fast ions inducing a strong drive for TAEs. For example, NBI ions will be injected at $\mathcal{E} = 80keV$, which gives the following estimates for the injected ion velocity and the Alfvén velocity : $v_{b0} = 3 \times 10^8 cm/s \gg v_{A0} \simeq 10^8 cm/s$, fast ion Larmor radius $\rho_{Lb}/a \simeq 1/4$, and drift orbit radial width $\Delta_b/a = (q/\epsilon)\rho_{Lb}/a \simeq 1/2$. In this work, TAEs in NSTX are analyzed using the improved NOVA-K code, which includes fast ion finite orbit width and Larmor radius effects to calculate the stability [13] and predicts the saturation amplitude for the mode using a quasilinear theory[14]. Then the ORBIT code is used[15] to estimate the effect of TAEs on fast neutral beam ions.

When NOVA-K is limited by applicability of its perturbative approximations, we use the nonperturbative fully kinetic code HINST[16], which stands for *high-n stability* code. This code is able to reproduce RTAE branches with arbitrary drive. It includes bulk plasma and fast particle Finite Larmor Radius (FLR) effects. Radiative damping supported by trapped electron collisional effects and ion Landau damping is also included. Even though HINST is able to reproduce robust solutions with high toroidal n numbers that have radially localized mode structures, it can be used for medium-n to low-n modes in the local version of the HINST without resolving two-dimensional ($2D$) structure. We will use HINST in this paper to analyze the observation of chirping frequency modes from TFTR and JT-60U tokamaks. Different scenarios and physical mechanisms are proposed to explain such experimental phenomena. Our approach is purely linear, however we can predict the response of the plasma to fast particles and with different fast particle distributions without discussing how a given distribution is formed. Such an approach includes the right physical mechanisms responsible for the frequency chirping in experiments. Note that nonlinear effects should be important and need to be considered, but it is not within the scope of this paper. Nonlinear evolution of a model bump on tail instability is able to demonstrate frequency chirping as was shown in Ref. [17]. However, the full picture may be obtained only by combining the nonlinear model with proper nonperturbative plasma dispersion analysis.

3

2 Perturbative TAE Analysis in NSTX

2.1 Linear Eigenmode Study

In the NOVA-K code calculations, the conservation of three particle integrals of motion is assumed, which are velocity v, magnetic moment $\mu = v_\perp^2/2B$, and toroidal canonical momentum P_φ. We analyzed four NSTX equilibria. The first equilibrium has a low central safety factor $q_0 = 0.4$, and $q_{edge} = 15$, which corresponds to the Time-dependent transp analysis code (TRANSP) [18] run #11112P60 with $\langle\beta\rangle \equiv 8\pi\langle p\rangle/\langle B^2\rangle = 10\%$ ($\beta_{tor} \equiv 8\pi\langle p\rangle/B_{\varphi 0}^2 = 34\%$). The second equilibrium has medium $q_0 = 0.7$, $q_{edge} = 16$ with $\langle\beta\rangle = 10\%$. The third and the fourth equilibria have high $q_0 = 2.8$, $q_{edge} = 12$ with high beta $\langle\beta\rangle = 15\%$ and medium beta $\langle\beta\rangle = 8\%$, respectively. Pressure and density profiles are presented in the form $P(\psi) = P(0)\left(1 - \psi^{1.03}\right)^{1.7}$, $n_e(\psi) = n_e(0)\left(1 - \psi^{1.62}\right)^{0.48}$ for low-q_0 and medium-q_0 cases, while for high-q_0 case we use $P(\psi) = P(0)\left(1 - \psi^{1.8}\right)^2$, $n_e(\psi) = n_e(0)\left(1 - \psi^{10}\right)^{0.12}$. The vacuum magnetic field is $B_0 = 0.3T$ at the geometrical axis.

Density and safety factor profiles are flat near the plasma center, creating an aligned gap along the minor radius. Calculations show that the Alfvén continuum gap is large, due to the effect of strong toroidal coupling and does not close at high beta $\beta \simeq 1$, so that TAEs can still exist. For each toroidal mode number n we found several TAE modes. Calculations also show that in NSTX, TAEs typically have very broad radial structure covering the whole minor radius. Thermal tail ions may be super-Alfvénic at energies $\mathcal{E}_i > 6keV$, which indicates that plasma ion ω_{*i} effects are important but, are neglected in our model. Figure 1 illustrates the gap structure, where the frequency of the continuum is shown as normalized to the Alfvén frequency $\omega_A = v_{A0}/q_{edge}R_0$, R_0 is the major radius of the geometrical center and v_{A0} is the Alfvén velocity evaluated with the central plasma mass density and magnetic field at the geometrical axis. We note that higher frequency gaps, i.e., gaps induced by non-circularity, are usually closed in NSTX plasma. Also note that high pressure leaves gaps open, allowing for global TAE to exist.

We performed calculations for toroidal mode numbers $n = 1, 3, 5, 7$. The following number of TAE modes were found: 6 modes for low-q_0, 22 modes for medium-q_0, 11 for high-q_0 high-β, and 8 for high-q_0 medium-β equilibria. Examples of two TAE mode structures are
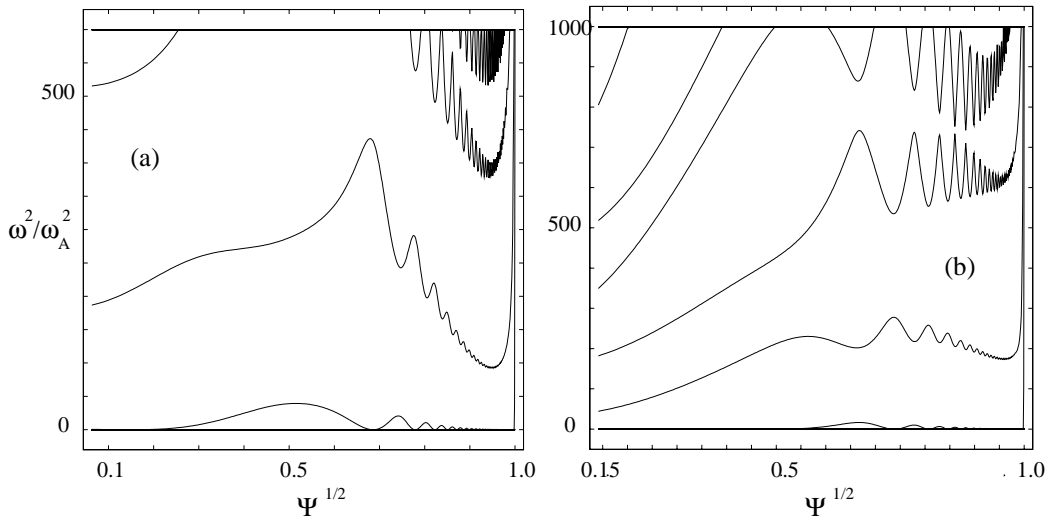
Figure 1: Alfvén continuum gap in NSTX plasma for $n = 3$ in medium-q_0 equilibrium with low ($< \beta >= 10\%$) and high ($< \beta >= 33\%$) plasma beta.

shown in Figure 2. The poloidal mode numbers for each harmonic are labelled according to the notations: 'A' corresponds to $m = -1$, 'B' is $m = 0$, 'C' is $m = 1$ and so on.

2.2   Stability Study

Our analysis of TAE stability in NSTX is perturbative with eigenmode structure calculated by the ideal MHD code NOVA [11] and with drive and damping calculated by the post-processor code NOVA-K[12]. The NOVA-K code was recently improved[13] to analyze the stability of Alfvén modes with arbitrary particle orbit width in general tokamak geometry. Trapped electron collisional damping is modified and includes not only trapped electron interaction with the parallel electric field[19], but also electron compression effects as well. TAE drive is induced by the pressure gradient of NBI ions, which are injected tangentially to the major radius with beam width roughly equal to one half of the minor radius. The distribution function of fast ions needs to be calculated separately and is beyond the scope of this work, so that we assume the distribution function of fast ions to be slowing down in energy with a Gaussian distribution in pitch angle $\lambda = \mu B_0 / E$, which is peaked at $\lambda = 0.3$ and has width $\Delta \lambda = 0.5$. Fast particle radial pressure profile is given by TRANSP for low-
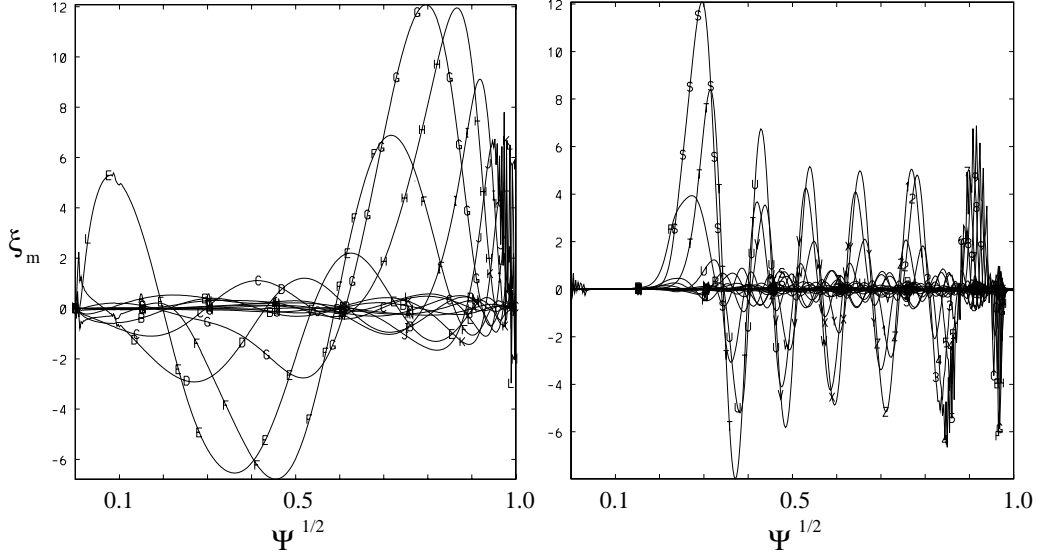
Figure 2: TAE mode structure for high-q_0 high beta NSTX plasma at $n = 1$ and $n = 5$.

and medium-q_0 equilibriums and is $P_b(\psi) = P_{b0}\left(1 - \psi^{1.33}\right)^{3.4}$ for high-q_0.

Table 1 summarizes the results of the stability study for $n = 1, 3, 5, 7$ modes. It shows the values of fast particle beta at the center, the number of stable and unstable eigenmodes for a given equilibrium, and the lowest critical fast particle beta when the mode can be unstable. In NSTX, linear perturbative calculations predict very strong drive for TAEs, which may be as high as $\gamma/\omega > 30\%$ and makes our perturbative approach inaccurate (but does not change the qualitative stability properties). The eigenmode structure and the eigenfrequency can be modified as compared to the MHD solution by fast particles during the mode nonlinear evolution. Another important result of our calculation is that NOVA-K predicts unstable modes with higher, $(n > 3)$, even without fast particles, but with the same thermal plasma parameters. The drive occurs because $\omega < \omega_{*i}$ and originates from the tail of the Maxwellian background ions, which at energies $\mathcal{E} \simeq 6keV$ have a velocity close to the Alfvén velocity. For such cases $(n = 5)$ the value of the critical beta of fast ions is zero as shown in the table. The parenthesis shows the lowest critical beam beta for the modes with thermal ion damping $(n \leq 3)$. The dominant damping mechanism is ion Landau damping for all the cases studied.

equilibrium	$\langle\beta\rangle, \%$	$\beta_b(0), \%$	# of stable modes	# of unstable modes	# of modes with $\gamma/\omega_A > 30\%$	lowest $\beta_{bcrit}(0), \%$
low-q_0	10	63	6	0	0	90
medium-q_0	10	11	19	3	0	9
high-q_0	15	> 22	6	5	6	0 (1)
high-q_0	8	> 10	5	3	2	0 (15)

Table 1: TAE stability analysis statistics and lowest fast ion critical beta for $n = 1, 3, 5, 7$ modes.

2.3   TAEs Effects on Fast Ions

The guiding center orbit code ORBIT[15] is used to calculate the effect of TAEs on fast particle confinement in NSTX. Because of strong poloidal harmonic coupling, each eigenmode has to be represented by many poloidal harmonics, which is a time consuming procedure for particle codes such as ORBIT. Thus, we consider $n = 1$ TAE with the highest drive for each equilibrium. For the analysis of two unstable TAEs, we choose $n = 1$ and $n = 3$. NOVA-K is capable of predicting TAE amplitude using quasilinear theory[13][14], and can be used to evaluate the TAE amplitude in NSTX plasma. As there are uncertainties in plasma parameters, we consider only the trend in the parametric dependence of the eigenmode amplitude. We found that typically the mode amplitude is at least an order of magnitude higher in NSTX than in TFTR for the same growth rate to the damping rate ratio. This is due to higher "effective" collisionality in NSTX. Based on NOVA-K calculations, we choose the TAE amplitude to have the same value for all eigenmodes with $\tilde{B}_\theta/B = 10^{-3}$. Table 3 shows the results of ORBIT calculation of beam ion loss fraction for low $q_0 = 0.4$, $\langle\beta\rangle = 10\%$ and high $q_0 = 2.8$, $\langle\beta\rangle = 15\%$ equilibria. Shown are total prompt losses which occur when no mode is present. The losses mostly occur during the first particle transit over the drift orbit. Also shown are total fast ion losses when one or two modes are included. In tokamaks at such TAE amplitudes resonances usually overlap and produce significant particle loss[20]. In NSTX, the large beam ion Larmor radii, the magnetic well near the center and strong edge poloidal magnetic field help to confine particles at high beta, so that TAEs do not

——	low-q_0	——		——	high-q_0	——
losses,%$\rightarrow$	prompt	$n = 1$ TAE		prompt	$n = 1$	$n = 1$ & $n = 3$
no FLR	9	11		1	2	
with FLR	29	31		24	30	35

Table 3: Particle losses as simulated by ORBIT in low- and high-q_0 equilibria

produce large additional losses. Note that we included FLR effect in the ORBIT code only approximately. At each step on a particle guiding center trajectory the Larmor radius ρ_b is evaluated. If a particle comes closer than ρ_b to the last flux surface it is considered lost. This may overestimate the losses as the Larmor radius may be smaller at the edge because of a stronger poloidal field at the edge.

3   Nonperturbative Mode Analysis of ICRH-driven Chirping Modes in TFTR

During ICRH of the H minority in TFTR experiments, Alfvén frequency modes down chirp on a time scale of $100 - 200 msec$ near the plasma core, as illustrated in Figure 3 for the shot #67630, where both reflectometer measurements of the plasma density fluctuations near the center and edge Mirnov coil magnetic fluctuation measurements were available[5]. First, the reflectometer picks up the signal, and then Mirnov coils start to measure the magnetic field edge perturbations, which implies the perturbation outward shift. Often H minority losses were seen at the plasma edge, which indicates increased particle transport during the chirping mode activity. After the chirping mode starts, other types of Alfvén mode activity can be observed with slightly evolving frequency. The latter may be identified as TAE. On the other hand, chirping modes are very similar to those observed in JT-60U experiments [21], so that the frequency chirp may be explained within linear theory [5].

TRANSP has been applied to model plasma behavior in this shot #73268. Basic plasma parameters for the time $t = 39.3sec$ were major radius $R_0 = 2.64m$, minor radius $a = 0.95m$, central plasma beta and density were $\beta_{pc}(0) = 1.1\%$ and $n(0) = 3.6 \times 10^{13} cm^{13}$, fast particle beta profile $\beta_H(0) = 5.8(1 - (r/a)^4)^4$. NOVA predicts a radially closed toroidal Alfvén gap for this case. The large H minority beta can not be considered a perturbation. NOVA
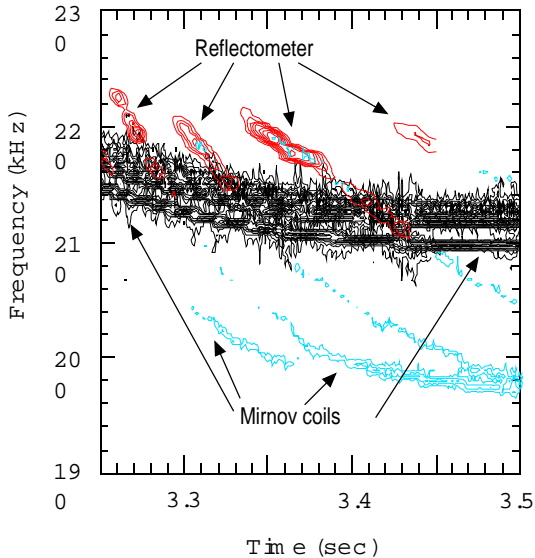
8

Figure 3: Chirping frequency modes from TFTR shot ICRF as seen by the reflectometer and Mirnov coil measurements.

predicts the solution for low plasma central beta as a Core Localized Mode (CLM), but fails to resolve mode for central plasma beta $\beta(0) > \beta_{cr} = 2.2\%$ because of a strong interaction of core localized TAE solutions with the lower continuum. The obtained β_{cr} from NOVA is much less than the predicted central total plasma beta by TRANSP $\beta(0) = \beta_{pc}(0) + \beta_H(0) = 6.9\%$.

New types of TAE branches are expected to exist in such plasma conditions and are known as RTAE[8]. RTAE can exist even inside the Alfvén continuum if the fast particle drive is strong enough to overcome the radiative continuum damping. At given plasma parameters near the plasma center with low shear, we can use only the local version of HINST, which produces only the mode frequency, the growth rate and the one-dimensional ($1D$) mode structure in the ballooning variables. Note that the global HINST $2D$ solution requires radial localization of the mode and high toroidal mode number n [16].

We found RTAE solutions using the HINST code with a fast particle distribution function taken as Maxwellian in velocity space and all particles assumed well trapped. The temperature of H minority ions was taken to be $300keV$. The results are shown in Figure 4 for $n = 7$. It is clearly seen that the frequency of the solution is below the lower gap boundary. This is also seen from Figure 5 where the RTAE frequency is shown at fixed minor radius
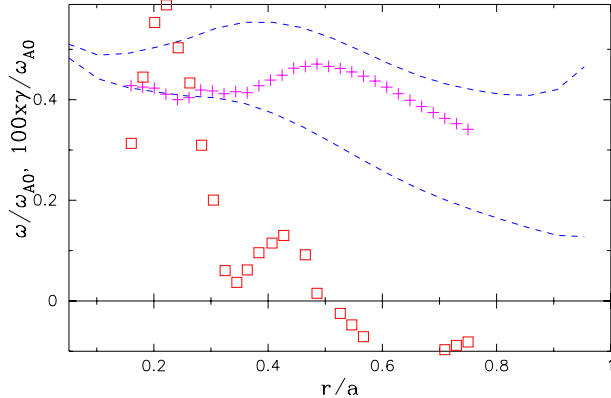
Figure 4: Local HINST results for RTAE frequency (shown as plus signs) and the growth rate (shown as open boxes) versus minor radius. Shown also is the toroidal gap envelope as dashed lines.

and fixed total plasma beta and varying the ratio of fast particle pressure to the background plasma pressure. At zero fast particle pressure the RTAE frequency goes even lower into the continuum and experiences strong damping. This is consistent with our conclusion based on NOVA calculations that the RTAE frequency is just below the lower gap.

To demonstrate the mode frequency chirping during the evolution of the q-profile between the sawteeth in ICRH TFTR discharges, we use a local version of HINST for different mode numbers $n = 6, 7, 8$. Fig.6 presents the radial dependence of the RTAE mode frequencies. To determine the radial position of RTAE, and thus the frequency at a given moment, we assume that RTAE has the same location as core localized TAE, which is given by the minor radius at $q(r/a) = q_{RTAE} = q_{TAE} = (m - 1/2)/n$. Thus $x_{RTAE} \equiv r/a = q^{-1}(q_{RTAE})$, where q^{-1} means the inverse function of q. A higher toroidal mode number is farther from the plasma center, as illustrated on Figure 7 at given $q_0 < 1$ and monotonic q-profile.

Finally, we superimpose the RTAE frequency versus minor radius dependence with the dependence $x_{RTAE} = q^{-1}(q_{RTAE})$ and calculate frequency time dependence assuming $q_0(t)$ is linear. Figure 8 shows the comparison of the measured frequency and HINST calculated frequency evolution. Two dependencies are qualitatively similar and have the same toroidal mode number time sequence. We note that the growth rate is of the order of $\gamma/\omega \simeq 2\%$, which is relatively low and may justify our linear approach against the nonlinear chirping
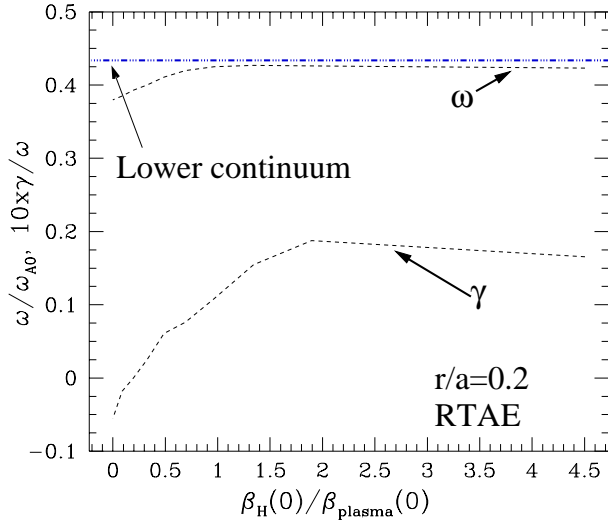
Figure 5: HINST RTAE solution frequency at minor radius $r/a = 0.2$ and the growth rate (as indicated) as a functions of minor radius. The RTAE frequency is below lower toroidal gap boundary and moves even lower if β_H goes to zero at fixed total plasma beta.
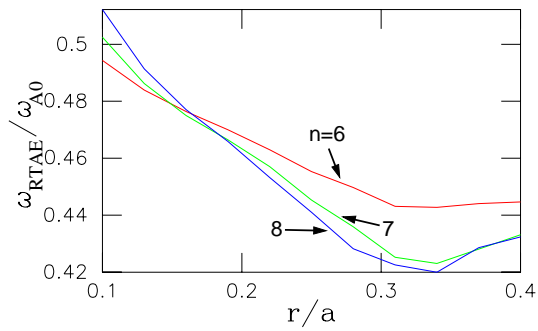

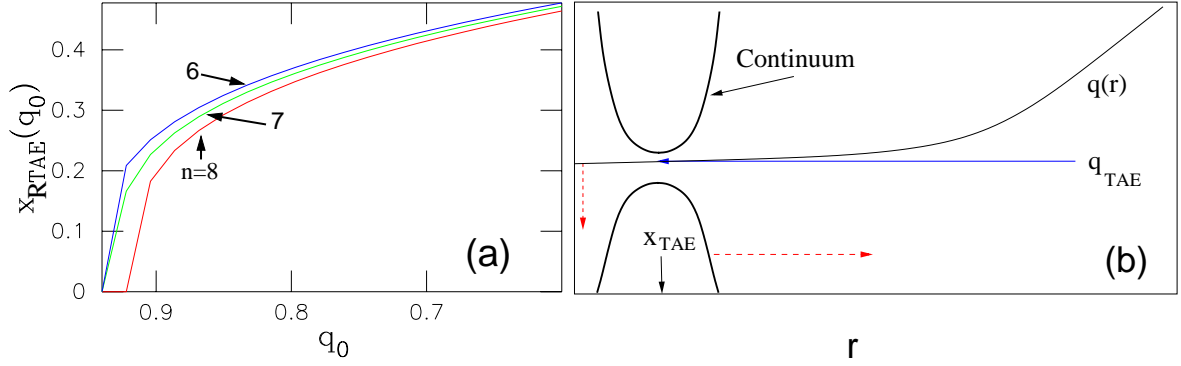Figure 6: RTAE frequency radial dependence for different toroidal mode numbers $n = 6, 7, 8$.

Figure 7: The radial location of the RTAE mode as a function of q_0 at a fixed q -profile (a) and a sketch (b), which illustrates the chirping mechanism through the mode location evolution as the q profile evolves and q_0 decreases.
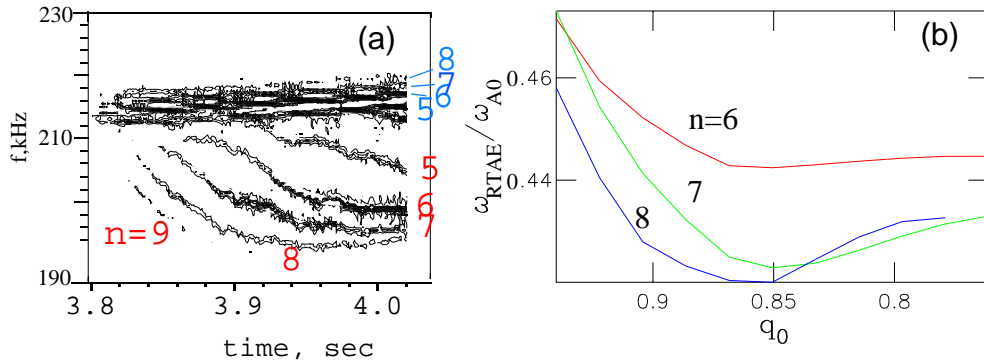
Figure 8: Measured evolution of the Mirnov coil oscillation frequency (a) vs. the HINST predicted RTAE frequency "evolution" (b) expressed as a function of central safety factor q_0.

12

mechanisms. Also, it is important to note that such analysis can be done only with the nonperturbative codes such as HINST. In this case, it is not due to the strong drive, but rather to the presence of a large number of fast particles, which changes the background plasma dispersion and creates a new RTAE branch. We conclude again that a more comprehensive code applicable for low to medium n number modes is needed. However, even now a local version is quite useful for the analysis of experimental data, especially with given uncertainties in the measurements of the q profile, fast particle pressure, and other plasma parameters. Local HINST analysis allows us to identify the modes and driving mechanisms and provides information about the possible mode location.

4 Negative NBI Excitation of Chirping Modes in JT-60U Experiments

4.1 Slowly Chirping Modes

Previously, the observation of different types of chirping modes in JT-60U tokamak plasmas were reported[6]. In that experiment, high energy $\mathcal{E}_{b0} = 360keV$ deuterium ions were injected tangentially into the plasma with a low toroidal magnetic field $B = 1.2T$, so that beam ions were super Alfvénic. Typically achieved fast particle central betas were comparable with the total plasma toroidal beta. Figure 9 presents the results of the measurements reported in Ref.[6]. One can see two kinds of mode activity, which will be discussed here. In the first one, the mode starts at $t \simeq 3.8sec$ with initial frequency $f = 30kHz$, and slowly chirps within $\sim 200msec$ to $f = 60kHz$ by the time $t = 4.0sec$. Relatively long chirping may be caused by the slow equilibrium evolution, rather than by nonlinear effects.

HINST can analyze high-n modes and, thus, may provide rather qualitative results for this case when only low-n oscillations are observed. Again we use a local version of HINST, which contains all the needed physics to model chirping modes and to reveal the basic physics responsible for the frequency chirp. We use TRANSP code [18] modeling for JT-60U discharge #32359, which computes NNBI ion beta and q-profiles at different times as shown on Figure 10. The beam ion beta profile evolution from Figure 10 shows the shift of the
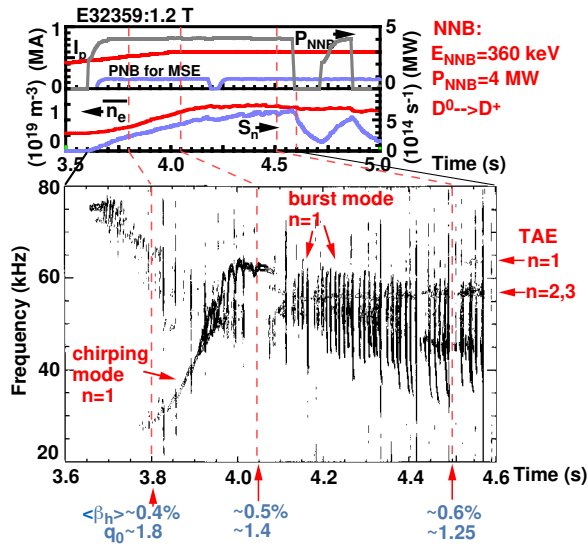
Figure 9: Slow and fast chirping mode activity measured by edge Mirnov coils in JT-60U NNBI injection experiments.
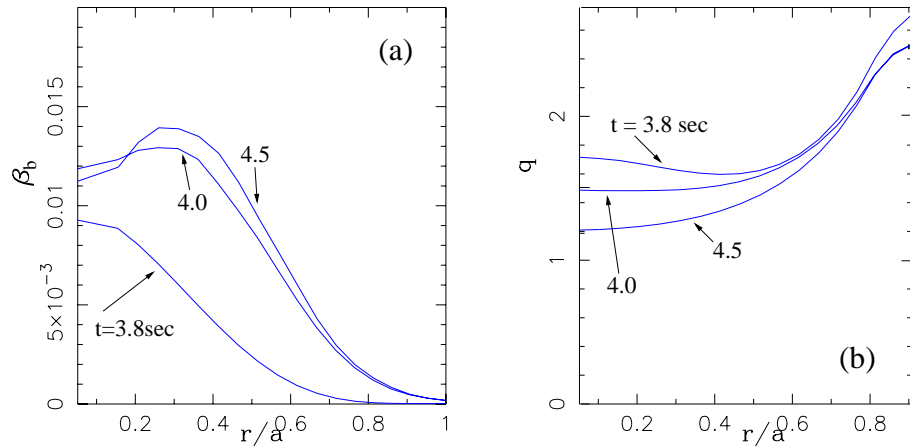

Figure 10: NNBI injected beam ion beta (a) and q profile (b) evolution for JT-60U shot #32359 as calculated by TRANSP.
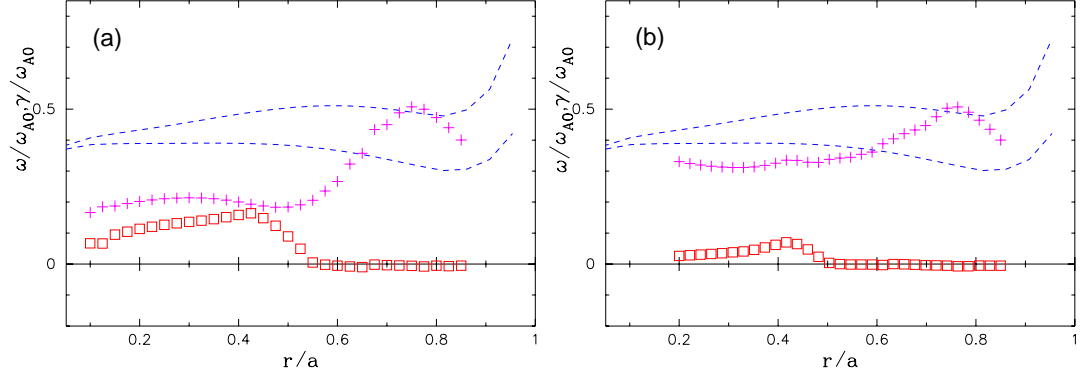
Figure 11: HINST analysis of the start of slow chirp $t = 3.8$. Two types of modes were found with the frequency shown as plus signs and the growth rates as open boxes. Strongest driven low frequency RTAE (a) has drive maximum at $r/a = 0.4$. High frequency RTAE (b) is less unstable. Shown also is the toroidal gap envelope represented by two curves.

fast particle pressure gradient along the minor radius. Total beam pressure is increased in time and is of the order of plasma beta $\beta_h(0) \sim \beta_p(0)$. The q-profile is evolving in a similar way as in ICRH experiments in TFTR. Note: presented beam ion beta profiles are rather qualitative and have not been benchmarked against other calculations. We use these profiles here to draw qualitative conclusions on the nonperturbative physics and its relation to the observed modes.

We found two different types of modes when the HINST code was applied for $n = 3$ at $t = 3.8 sec$, i.e., when the slow chirping mode was first observed. Figure 11 shows the HINST results as dependencies of the frequency and the growth rate on the minor radius.

Lower frequency mode is close to the kinetic ballooning mode (KBM) branch. The KBM is stable without fast particles, as can be seen in Figure 12. Also, calculations show the mode structure in the ballooning space, in η variable. The mode structure is broad [see Fig.13(a)], reflecting its kinetic nature and probably singular behavior in the radial direction. When the fast particle beta is introduced, the mode becomes localized in η [Figure 13(b)] and has finite growth rate. When fast particle beta is increased, the low frequency mode becomes more localized in η, as shown in Figure 14(a), which means that it has strong ballooning structure in real space. Higher frequency RTAE is closer to the TAE in frequency [see Figure 11(b)] and in mode structure [see Figure 14(b)]. The most unstable mode is the low frequency
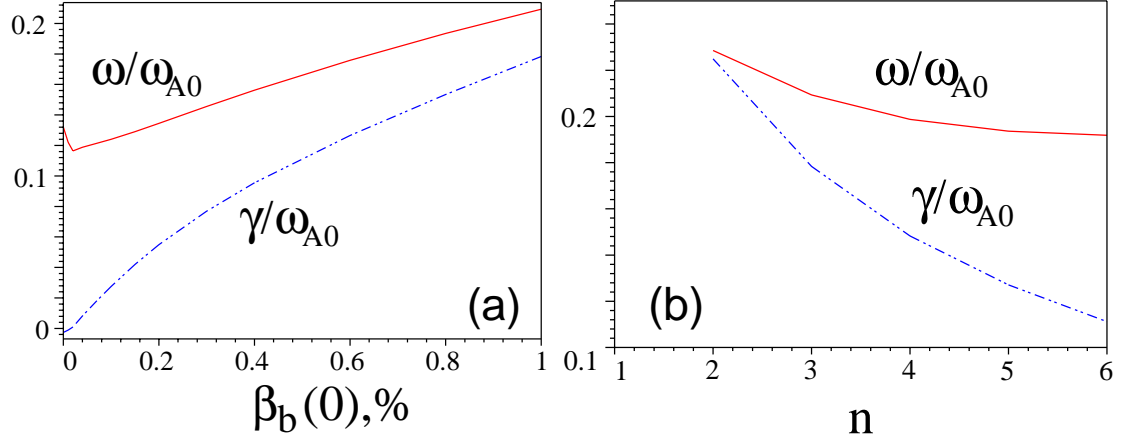
15

Figure 12: Properties of RTAE as dependencies of its frequency and growth rate on fast particle beam ion beta (a) and toroidal mode number n (b).
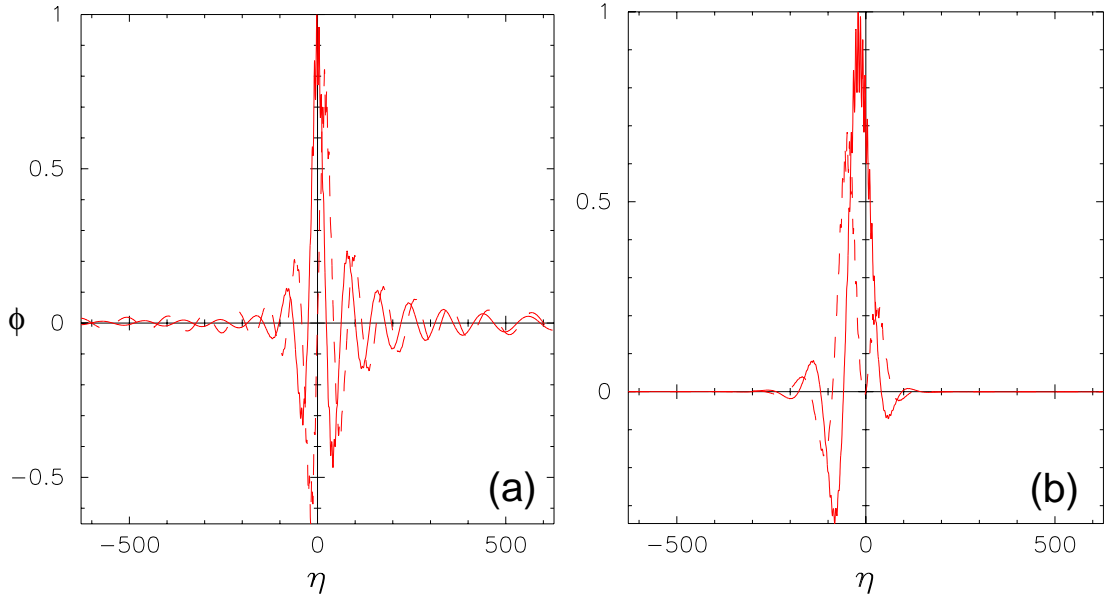

Figure 13: Ballooning structure of KBM at zero β_b (a), which transforms into the low frequency RTAE as fast particle beta increases. RTAE is more localized near the origin ballooning structure at $\beta_b(0) = 0.04\%$.
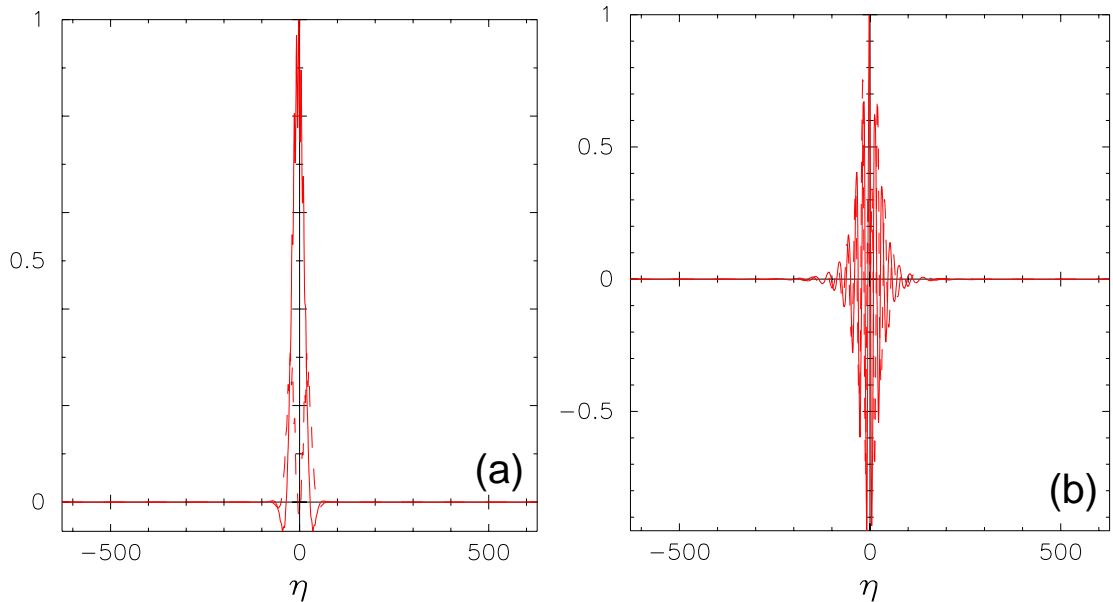
Figure 14: Low (a) and high (b) frequency RTAE ballooning structure at $\beta_b(0) = 0.4\%$.

RTAE and thus is expected to be excited first. Its frequency increases by $\sim 50\%$ when fast particle pressure is building up [see Figure 12(a)]. HINST predicts frequency change for $t = 3.8sec$ plasma parameters from $f = 17kHz$ to $f = 30kHz$ with fast particle beta at the center evolving from $\beta_b(0) = 0\%$ to $\beta_b(0) = 1.\%$. The lowest n number modes are the most unstable [Figure 12(a)], which agrees with experimental observation of the lowest n numbers $n = 1 - 2$.

Similar analysis performed at $t = 4.0sec$ is illustrated in Figure 15. With time, the fast particle beta profile becomes broader in radial direction so that the region of strongest gradient is moving outwards. Both low-frequency and high-frequency RTAEs merge into one branch at $r/a > 0.55$. The maximum growth rate is shifted to $r/a = 0.55$ with a higher mode frequency. HINST predicts the frequency of RTAEs for this case to be $f = 50kHz$, which is increased due to the higher beta and stronger shear at larger minor radius.
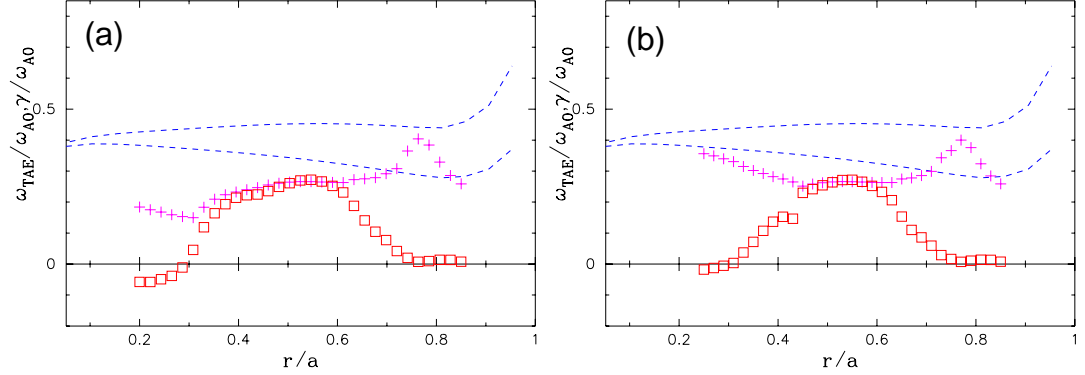
Figure 15: HINST analysis for $t = 4.0 sec$ shows two branches, low (a) and high (b) frequency RTAEs, which merge into one at $r/a > 0.55$.

4.2 Fast Chirping Modes

Fast chirping modes at $t = 4.0 - 4.5 sec$ have a characteristic time scale of $t = 3 - 5 msec$. We argue that it can not be related to the slow equilibrium changes, such as considered above. Detailed modeling of fast chirping modes needs to include both the nonlinear wave particle interaction and correct nonperturbative plasma response to the evolving beam distribution. Simple mode dispersion was included in the model of Ref.[17], where it was shown that fast chirping can be expected for strongly driven modes with evolving frequencies with time dependecies $f \sim \sqrt{t}$. Without a correct model for the nonlinear wave particle interaction, we can only demonstrate the response of the plasma+beam system to different fast particle distributions and thus propose the physical mechanism responsible for the fast frequency chirp.

We base our model on the following. Repetitive chirping modes provide transport of fast beam ions. All newly injected beam particles are alike, which means that almost all of them are transported from the region where the RTAE becomes unstable. We suggest that such a region can be the region with the largest linear growth rate, which is at the minor radius $r/a = 0.55$. Note that for $t = 0.45$, the fast particle beta profile is similar to the one at $t = 4.0 sec$. The beta of the beam particles in that region, having beam-like velocity distribution, which we call region 1, can be estimated as $\beta_{b1} = \beta_{b0} * \tau_{chip}/\tau_{se}$, where β_{b0} is equilibrium unperturbed beta of slowing down beam ions predicted by TRANSP code,
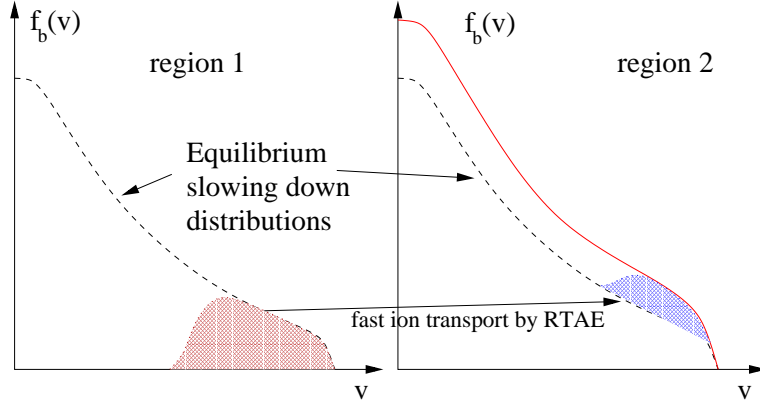
18

Figure 16: Schematic of the fast particle distributions in region 1, where RTAE is excited and region 2, where RTAE disappears. Shaded area in region 1 is beam-like distribution used in HINST calculations. Solid curve in region 2 is resulting slowing down distribution function.

τ_{chirp} is period between the chirping mode activity, and τ_{se} is slowing down time. From the TRANSP results we estimate the ratio $\tau_{chirp}/\tau_{se} = 1/4$. The mode stabilizes when it moves to such a radial position when the particles it carries goes out of the resonance. In that region (region 2), fast particles have a modified slowing down distribution. Thus, if we show that the frequency of the RTAE is sensitive to the type of the distribution function, then the physical picture we consider can provide the basis for the observed frequency chirp. The fast ion distributions in regions 1 and 2 are illustrated in Figure 16.

We choose the most unstable location for the RTAE $r/a = 0.55$ and vary the distribution function, which is allowed in the HINST code, so that we may have both beam like distribution and the slowing down distributions at the same time. The RTAE frequency is less sensitive to r/a than to the distribution function change (see Figure 15). Simulation of the RTAE frequency sensitivity to the distribution function is shown in Figure 17. We changed the distribution from the beam like to the slowing down distribution with the fast particle beta given by $\beta_b = \kappa\beta_{b1} + (1 - \kappa)\beta_{b0}$. Indeed we can expect around a 20% frequency change when particles are transported by RTAE radially. This is in qualitative agreement with the amount of the observed fast frequency chirp. Interesting to note that at fast particle beta given by the calculated ratio $\tau_{chirp}/\tau_{se} = 1/4$ the RTAE is close to the instability threshold
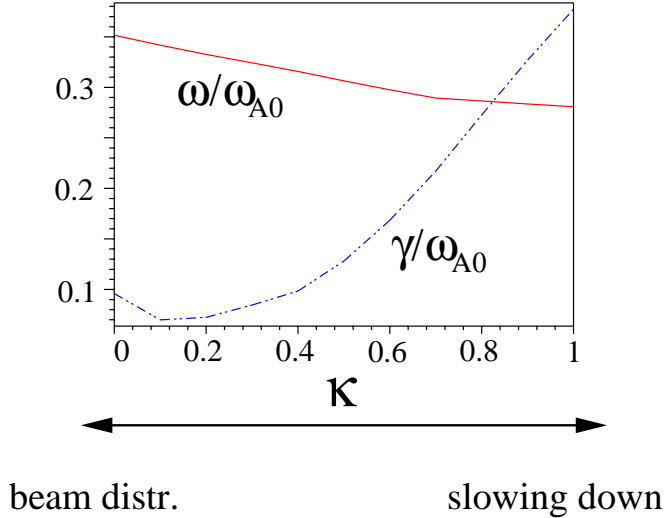
19

Figure 17: RTAE frequency is sensitive to the type of distribution function and changes within 20% when the distribution is changed from beam-like distribution to the slowing down distribution.

and has relatively low growth rate, which ultimately supports our model.

5 Summary

Many TAEs may be unstable in NSTX. TAEs are found to have a global radial structure. The Alfvén continuum gap exists even at high plasma beta, with TAE modes present. TAEs may have strong growth rate $\gamma/\omega > 30\%$, which requires nonperturbative codes for more accurate calculations. Single- and two-mode calculations predict the highest beam ion loss in high beta high-q_0 plasmas $\sim 35\%$ of the NBI ion population with FLR effects included, where most of the losses are prompt losses (24%). Good fast ion confinement is observed in high beta plasmas because of the presence of the magnetic well and strong poloidal field at the edge.

HINST analysis of the experimental data from tokamaks such as TFTR and JT-60U suggests that modes with a strong drive from fast particles are common and may be dangerous for energetic particle confinement in a reactor. Agreement is achieved for the modeling of

slowly chirping modes in TFTR where a slow q-profile evolution is shown to produce the frequency chirp. Slow chirps may also be caused by the slow change in fast particle pressure profile and was illustrated for the JT-60U experiments with NNBI heating. More complete modeling resolving the mode structure is required to confirm this mechanism. The third mechanism responsible for the mode chirping is the fast change of the fast particle distribution function during the nonlinear mode evolution. The amount of the frequency chirp is consistent with that experimentally measured.

A more comprehensive code which includes a nonperturbative treatment of fast particle contribution is needed for low-n mode analysis and for more accurate modeling of the linear and nonlinear interaction.

References

[1] C. Z. Cheng, L. Chen and M. S. Chance, Ann. Phys. **161** 21 (1984).
   C. Z. Cheng and M. S. Chance, Phys. Fluids **29** 3695 (1986).

[2] R. Nazikian, *et.al.,* Phys. Plasmas, **5** 1703 (1998).

[3] W. W. Heidbrink, Plasma Phys. Control. Fusion, **37** 937 (1995).

[4] K. G. McClements, *et.al.,* Plasma Phys. Control. Fusion **41** (1999) 661.

[5] S. Bernabei, *et.al.,* Phys. Plasmas, **6** (1999).

[6] S. Kusama, IAEA-98.

[7] M. Takechi, K. Toi, S. Takagi, *et.al.* Phys. Rev. Lett., **83** 312 (1999).

[8] C. Z. Cheng, N. N. Gorelenkov, and C. T. Hsu, Nucl. Fusion **35**, 1639 (1995).

[9] L. Chen, Phys. Plasmas **1**, 1519 (1994). F. Zonca and L. Chen, Phys. Plasmas **3** (1996).

[10] *see posters by* J. Menard, D. Darrow, R. Kaita*, this conference.*

[11] C. Z. Cheng, and M. S. Chance, J. Comput. Phys. **71**, 124 (1987).

[12] C. Z. Cheng, Phys. Reports, **211**, 1 (1992).

[13] N. N. Gorelenkov, C. Z. Cheng, G. Y. Fu, Phys. Plasmas **6** 2802 (1999).

[14] N. N. Gorelenkov, *et.al.,* Phys. Plasmas, **6** 629 (1999).

[15] R. B. White, M. S. Chance, Phys. Fluids **27** 2455 (1984).

[16] N. N. Gorelenkov, C. Z. Cheng, and W. M. Tang, Phys. Plasmas, **5**, 3389 (1998).

[17] H. Berk, B. Breizman, *et.al.,* Plasma Physics Reports, **23** 778 (1998).

[18] R. V. Budny, *et. al.,* Phys. Plasmas **3** 4583 (1996).

[19] G. Y. Fu, *et. al.,* Phys. Fluids **5** 4040 (1993).

[20] C. T. Hsu, D. J. Sigmar, Phys. Fluids B **4** 1492 (1992).

[21] G. Kramer, C. Z. Cheng, G. Y. Fu, *et.al.* Phys. Rev. Letter **83** 2961 (1999).

[22] N. N. Gorelenkov, *et.al.,* In Proc. 17th IAEA Fusion Energy Conf., Yokohama, 1998, paper IAEA-F1-CN-69/THP2/21.